

Transfer operator approach on three-dimensional quantum billiards with SO(2) symmetry

Cheng-Hung Chang

Physics Division, National Center for Theoretical Sciences, 101, Section 2 Kuang Fu Road, Hsinchu 300, Taiwan

(Received 15 August 2002; revised manuscript received 6 January 2003; published 7 April 2003)

This work demonstrates the application of Bogomolny's transfer operator method on three-dimensional dynamics. Motivated by experimental observations of lenslike metal clusters, the quantum billiards bounded by a flat bottom and an upper surface with SO(2) symmetry are studied. A precise determination of the energies with error less than 0.05% and exact predicted degeneracies in the special case of the half-sphere billiard confirm the efficiency of this method. Furthermore, the spectra and degeneracies of lens billiards with varying heights are explicitly determined.

DOI: 10.1103/PhysRevE.67.046201

PACS number(s): 05.45.Mt, 03.65.Sq, 05.45.Pq

I. INTRODUCTION

Bogomolny's transfer operator method is a well-known quantization method in the study of quantum chaos [1], along with other methods such as Gutzwiller's trace formula and dynamical ζ function, which relate the energy spectrum of a quantum system to its classical dynamical system [2]. This method is not only conceptually appealing, because of its connection between the quantum and classical worlds, but also practically important, because it provides an efficient method of quantization. The basic idea of this method is to convert the eigenvalue problem of a Hamiltonian in a k -dimensional real space to the eigenvalue problem of a corresponding transfer operator on a $(k-1)$ -dimensional Poincaré section, in the spirit of the boundary integral method [1], from which the transfer operator method was derived. This conversion considerably reduces the dimension in numerical work and hence the computational effort, especially for asymmetric systems, in which the Hamiltonian cannot be factorized. Moreover, the transfer operator is relatively easy to construct, since for proper Poincaré sections, it is defined only on a finite number of classical trajectory segments, in contrast to most semiclassical methods based on infinitely many periodic orbits, which are difficult to determine systematically, e.g., due to the exponentially proliferating number of orbits with their length in ergodic systems [2,3]. Such a complex application procedure can be seen in the example of applying the trace formula to the three-dimensional (3D) Sinai billiard [4].

Despite these two advantages, the transfer operator method is correct only up to \hbar^2 in the stationary phase approximation. It is exact only in the semiclassical limit $\hbar \rightarrow 0$ and a general error estimation for finite $\hbar > 0$ is absent. This fact raises the question of how reliable this method is in practice. This question has been clarified for various systems, to which the transfer operator has recently been applied, including billiards with hard boundaries such as rectangular billiards [5], Limaçon billiards [6], circle billiards [7,8], annulus billiards [9,8], triangular billiards [10], wedge billiards [7,11] and systems under potentials such as the Coulomb potential [8], harmonic oscillators [8,12], the Nelson potential [13], and geodesic flow on Riemann surfaces of constant negative curvature [14]. However, the transfer operator in all of these studies were constructed on two-dimensional (2D)

dynamics (to the best of the author's knowledge). The only one 3D system studied has SO(3) symmetry and was reduced to a 2D problem in the investigation [8].

The current work demonstrates the application of the transfer operator method on 3D trajectories. The geometry is motivated by recent experimental observations of various metal clusters shaped like lenses [15]. A peculiar phenomena exhibited in several of these clusters is the magic size of the clusters, due to particularly stable numbers of atoms in the clusters. This result is attributed to a combination of different effects, among which the quantum size effect plays an essential role. The simplest model for this effect in these clusters is that of a single particle confined within a 3D quantum billiard bounded by a flat bottom and an upper surface with SO(2) symmetry (see an example in Fig. 1). The application of the transfer operator method will be presented on those geometries.

The SO(2) symmetry enables the reduction of the Hamiltonian from a 3D problem to a 2D problem. This reduction provides analytical solutions in the special case of the half-sphere quantum billiard. The validity of applying the transfer operator method in this special case is confirmed by precise energy determination (decreasing error at least less than 0.05% by increasing the dimension of the discretized transfer

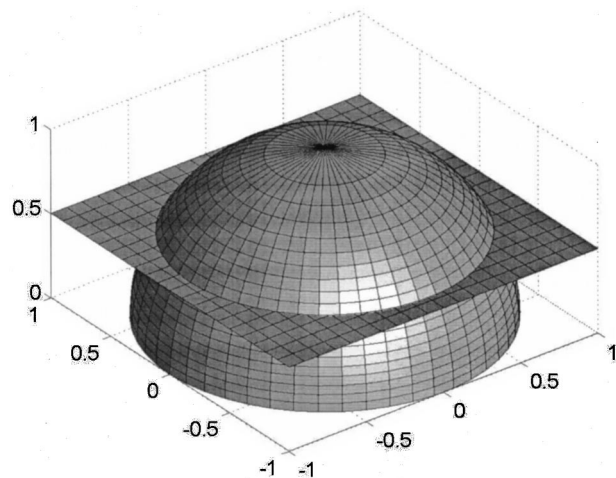


FIG. 1. A lens quantum billiard is a particle confined by a cut plane and the upper part of a half-sphere above this cut plane. The particle inside is reflected elastically by the hard boundary.

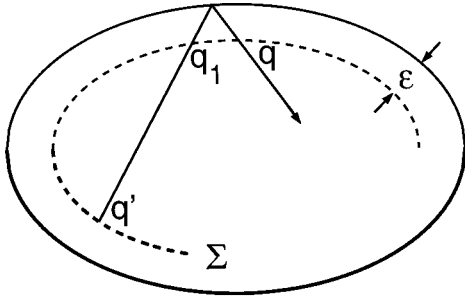


FIG. 2. Poincaré section Σ and crossing points q' and q in the transfer operator method.

operator) and correct prediction of degeneracies. Furthermore, the energy spectra and the degeneracies of lens quantum billiards with different heights are determined.

II. THE TRANSFER OPERATOR METHOD

Consider a particle with energy E , moving in a k -dimensional real space. Select a $(k - 1)$ -dimensional Poincaré section (PS) Σ in this space, such that almost all classical trajectories pass this section. Figure 2 shows the example of a 2D billiard ($k = 2$) with the boundary X (solid curve) and a PS Σ (dashed curve) with a distance ε far from X . Beginning with an initial position q' on Σ pointing towards the inner side of Σ , the next crossing point is the next point at which the trajectory crosses Σ and points towards the same side of Σ as it did at q' . Accordingly, the next crossing point after q' in Fig. 1 is q , not q_1 .

The transfer operator $\mathcal{T}(E)$ is defined as the integral operator [1],

$$\mathcal{T}(E)\psi(q) = \int_{\Sigma} T(q, q', E)\psi(q')dq',$$

acting on some function $\psi(q')$ on Σ . The integral kernel

$$T(q, q', E) = \sum_{\text{class. traj.}} \frac{1}{(2\pi i \hbar)^{(k-1)/2}} \times \sqrt{\left| \frac{\partial^2 S(q, q', E)}{\partial q \partial q'} \right|} \times \exp[iS(q, q', E)/\hbar - i\nu\pi/2] \quad (1)$$

is defined as the sum over all possible classical trajectories from the initial point $q' \in \Sigma$ to the final point $q \in \Sigma$ in the real space at energy E without any crossing points in between. The function $S(q, q', E)$ in Eq. (1) is the action along the trajectory from q' to q and the Maslov index ν is related to the number of the points, at which the semiclassical approximation is not valid [1]. In billiard systems with a hard boundary, this index is double the number of reflection points of the trajectory between q' and q at the boundary. In the following, the distance ε is assumed to be infinitely close to zero, such that the points $q', q \in \Sigma$ can be regarded as on the billiard boundary, when the length of the trajectory segment

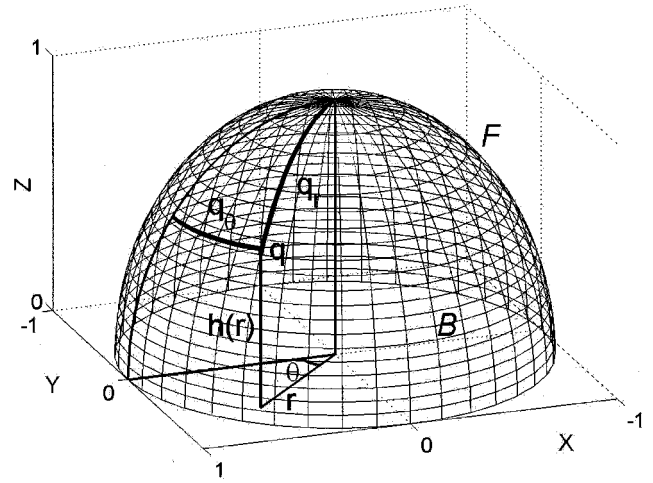


FIG. 3. Representation of q in the coordinate system (r, θ) on B and the coordinate system (q_r, q_θ) on F .

between q' and q is calculated. But one should keep in mind that $\varepsilon \neq 0$ when counting the reflection points at the boundary between q' and q . According to Bogomolny's theory [1], in the semiclassical limit $\hbar \rightarrow 0$, the zeros of the Fredholm determinant,

$$\det[1 - \mathcal{T}(E)] = 0,$$

of the transfer operator $\mathcal{T}(E)$ are the energies of the corresponding quantum system.

III. THREE-DIMENSIONAL QUANTUM BILLIARDS WITH SO(2) SYMMETRY ON A PLATE

One of the frequently observed shapes of the 3D metal clusters can be described by the quantum billiard, bounded by a flat circular bottom B on the xy plane and an upper surface F with SO(2) rotational symmetry. A point $q(x, y, z)$ on F can be represented in the polar coordinate $q(r, \theta)$ on B , with

$$x = r \cos(\theta), \quad y = r \sin(\theta), \quad \text{and} \quad z = h(r),$$

where r refers to the distance from the origin to the point on B projected down from $q \in F$, θ represents the angular variable of this projected point, and $h(r)$ stands for the height of q at radius r (Fig. 3). Alternatively, the point q can be represented in the coordinate $q(q_r, q_\theta)$ on the surface F , characterized by the path length q_r on F from the center of F to q and the path length q_θ on F in the rotational direction (Fig. 3). Variables on these two coordinate systems are related by

$$q_r = \int_0^r \sqrt{1 + \left(\frac{\partial}{\partial r'} h(r') \right)^2} dr', \quad q_\theta = r\theta. \quad (2)$$

Select a PS Σ inside the billiard and infinitesimally close to F . Given an initial point q' and a final point q on Σ , there exist only two trajectories from q' to q without other cross-

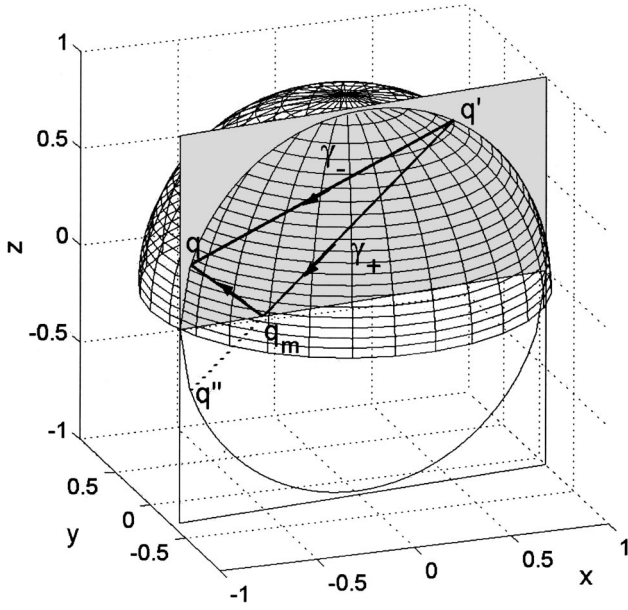


FIG. 4. Two trajectories γ_{\pm} from the initial point q' to the final point q on a PS Σ in the half-sphere billiard system.

ing points in between. Figure 4 shows an example in which F is a half sphere. The first trajectory γ_- is reflected by the upper boundary F once, shortly before it reaches q . The second trajectory γ_+ is reflected once at q_m by the bottom B and once by F , shortly before arriving at q . The trajectory segment $qq_m \cup q_m q'$ of γ_+ is of the same length as the segment $q''q_m \cup q_m q'$ from q' to the image q'' of q reflected by the mirror B .

All points q , q' , q'' , q_m , and trajectories γ_{\pm} are on the same plane (the gray plane in Fig. 4). Thus, the length of γ_{\pm} from $q'(r', \theta') = q'(x', y', z')$ to $q(r, \theta) = q(x, y, z)$ can be easily calculated:

$$l_{\pm}(q, q', E) = \sqrt{(x-x')^2 + (y-y')^2 + (z \mp z')^2} \\ = \sqrt{\xi_1 \mp \xi_2},$$

with

$$\xi_1 = r^2 - 2rr' \cos(\theta' - \theta) + r'^2 + h(r)^2 + h(r')^2$$

$$\xi_2 = 2h(r)h(r').$$

Changing variables in the action

$$S_{\pm}(q, q', E) = \sqrt{2\mu E} l_{\pm}(q, q', E)$$

from (r, θ) to (q_r, q_{θ}) by relations (2) and deviating $S = S(q(q_r, q_{\theta}), q'(q'_r, q'_{\theta}), E)$ by q_r and q_{θ} , respectively, q'_r and q'_{θ} yields

$$\det \frac{\partial^2 S}{\partial q \partial q'} = \det \begin{pmatrix} \frac{\partial^2 S}{\partial q_r \partial q'_r} & \frac{\partial^2 S}{\partial q_r \partial q'_{\theta}} \\ \frac{\partial^2 S}{\partial q_{\theta} \partial q'_r} & \frac{\partial^2 S}{\partial q_{\theta} \partial q'_{\theta}} \end{pmatrix} \\ = \frac{\partial^2 S}{\partial q_r \partial q'_r} \frac{\partial^2 S}{\partial q_{\theta} \partial q'_{\theta}} - \frac{\partial^2 S}{\partial q_r \partial q'_{\theta}} \frac{\partial^2 S}{\partial q_{\theta} \partial q'_r}.$$

In concave billiards, or billiards wherein the angle between F and B inside the billiard exceeds $\pi/2$, the so-called ghost trajectories must be taken into account. Please refer to [1] for further detail. The Maslov index ν_- for γ_- is 2 and ν_+ for γ_+ is 4, since the trajectories γ_{\pm} from q' to q are reflected once by boundary F and twice by $F \cup B$, respectively. Consequently, kernel $T(q, q', E)$ of $\mathcal{T}(E)$ in Eq. (1) is explicitly determined by considering all quantities discussed above, where the sum in Eq. (1) includes only two trajectories γ_{\pm} .

Next the section Σ is discretized into N cells, in which the n th cell has the area Δ_n . Under the basis $\{\psi_n\}$ with

$$\psi_n(q) = \begin{cases} \frac{1}{\sqrt{\Delta_n}} & \text{for } q \in n\text{th cell} \\ 0 & \text{otherwise,} \end{cases}$$

the transfer operator \mathcal{T} is discretized into an N -dimensional matrix with entries

$$\mathbf{T}_{\alpha\beta} = \frac{\Delta_{\beta}}{2\pi i \hbar} \sum_{\gamma_{\pm}} \sqrt{\left| \det \left(\frac{\partial^2 S(q_{\alpha}, q'_{\beta}, E)}{\partial q_{\alpha} \partial q'_{\beta}} \right) \right|} \\ \times \exp[iS(q_{\alpha}, q'_{\beta}, E)/\hbar - i\nu\pi/2], \quad (3)$$

where q_{α} is the center point of the α th cell.

For the systems with $SO(2)$ symmetry considered here, the basis $\{\psi_n\}$ can be explicitly selected as follows. First, the surface F is divided into n_r stripes $F^{(i)}$, $i = 1, \dots, n_r$. The i th stripe $F^{(i)}$ is bounded by two cylinders centered at the z axis with radii r_{i-1} and r_i , where $r_0 = 0$ and $r_{i-1} < r_i$. Figure 5 shows the example of a half sphere divided into $n_r = 3$ stripes, which are bounded by the cylinders with radii r_0, r_1, r_2 , and r_3 ($r_0 = 0$). Radii r_i 's are selected such that the widths

$$L(r_{i-1}, r_i) := \int_{r_{i-1}}^{r_i} \sqrt{1 + \left(\frac{\partial}{\partial r'} h(r') \right)^2} dr' \quad (4)$$

of all stripes $F^{(i)}$ along the q_r direction are equal. The area of the i th stripe $F^{(i)}$ constructed in this way is then

$$A^{(i)} = 2\pi \int_{r_{i-1}}^{r_i} r' \sqrt{1 + \left(\frac{\partial}{\partial r'} h(r') \right)^2} dr'.$$

Next, the first stripe $F^{(1)}$ (in fact a hat) is divided into four cells $F^{(1,j)}$, $j = 1, \dots, 4$, of equal area $\Delta = A^{(1)}/4$. The i th

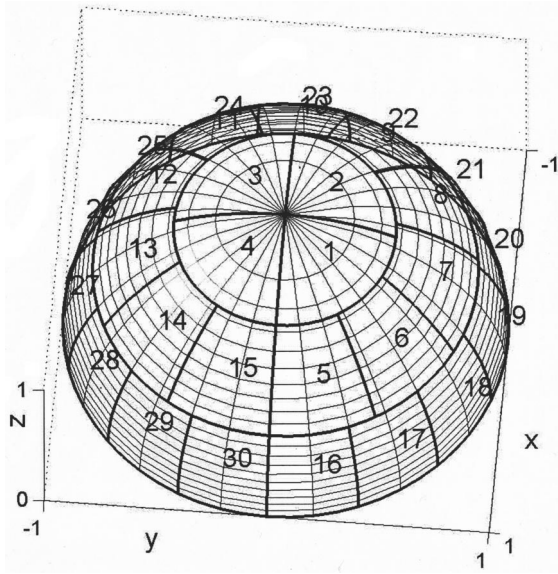


FIG. 5. Discretization of a half-sphere billiard with the height function $h(r) = \sqrt{1-r^2}$, the stripe number $n_r=3$, and the cell number $N=30$. The first stripe $F^{(1)}$ (in fact a hat) consists of four cells—1, 2, 3, and 4. The second stripe $F^{(2)}$ consists of 11 cells—from 5 to 15. The third stripe $F^{(3)}$ consists of 15 cells—from 16 to 30.

stripe $F^{(i)}$ is divided into $n_{\theta,i}$ cells such that the cell area $A^{(i)}/n_{\theta,i}$ is the closest value to Δ . Accordingly, the whole surface F is a union of all cells $F^{(i,j)}$,

$$F = \bigcup_{i=1}^{n_r} \bigcup_{j=1}^{n_{\theta,i}} F^{(i,j)}.$$

These cells $F^{(i,j)}$ are ordered from the first to the n_r th stripe counterclockwise, as shown in Fig. 5, where the first, second, and third stripe consist of $n_{\theta,1}=4$, $n_{\theta,2}=11$, and $n_{\theta,3}=15$ cells, respectively. The total number $N = \sum_{i=1}^{n_r} n_{\theta,i}$ of the cells, uniquely determined by n_r , is the dimension of the basis $\{\psi_n\}$ and of the discretized matrix $\mathbf{T}_{\alpha\beta}$, which equals 30 in the example in Fig. 5. The region of the k th cell, $k = j + \sum_{\alpha=1}^{i-1} n_{\theta,\alpha}$, in the i th stripe and the j th position, is represented by the half-open set

$$r \in [r_{i-1}, r_i) \quad \text{and} \quad \theta \in \left[(j-1) \frac{2\pi}{n_{\theta,i}}, j \frac{2\pi}{n_{\theta,i}} \right)$$

in the polar coordinate system (r, θ) , with the area $\Delta_k = F^{(i)}/n_{\theta,i}$ and its center point is located at

$$q \left(\bar{r}, \left(j - \frac{1}{2} \right) \frac{2\pi}{n_{\theta,i}} \right),$$

where the center position $\bar{r} \in [r_{i-1}, r_i)$ of the i th stripe in q_r direction satisfies $L(r_{i-1}, \bar{r}) = L(\bar{r}, r_i)$. In fact, the center point \bar{r} can be replaced by an arbitrary point $\bar{r}' \in [r_{i-1}, r_i)$ in the numerical approximation, because the discretized matrix $\mathbf{T}_{\alpha\beta}$ under different choice of \bar{r}' approaches the same operator \mathcal{T} by increasing cell number N .

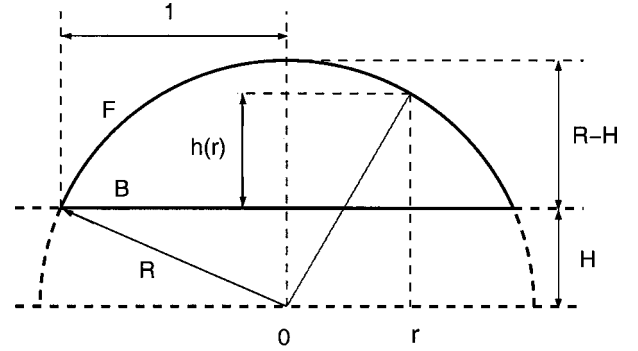


FIG. 6. Profile of lens quantum billiards bounded by a bottom (solid line) and an upper surface (solid arc) with width H .

The construction discussed so far is general and valid for all billiards bounded by a flat bottom and an upper surface with $SO(2)$ symmetry. The following applies this construction to the special case of lens quantum billiards, in which the upper bound F is part of a sphere.

IV. LENS QUANTUM BILLIARD

Consider a 3D billiard with $SO(2)$ symmetry described by the height function

$$h(r) = \sqrt{1+H^2-r^2} - H, \quad (5)$$

parametrized by a width H indicated in Fig. 6. The radius of the circular bottom B of this billiard specified by Eq. (5) remains 1 as H varies. For $H=0$, which implies $R=1$, the shape described by Eq. (5) is a half sphere. Figure 7 plots the absolute value of the Fredholm determinant $|\det[1 - \mathcal{T}(E)]|$ with a matrix dimension $N=395$, obtained by setting $\mu=1$ and $\hbar=1$ in Eq. (3).

The n th zero E_n of the function $\det[1 - \mathcal{T}(E)]$, with $E_n < E_{n+1}$, is the n th approximated energy of the half-sphere

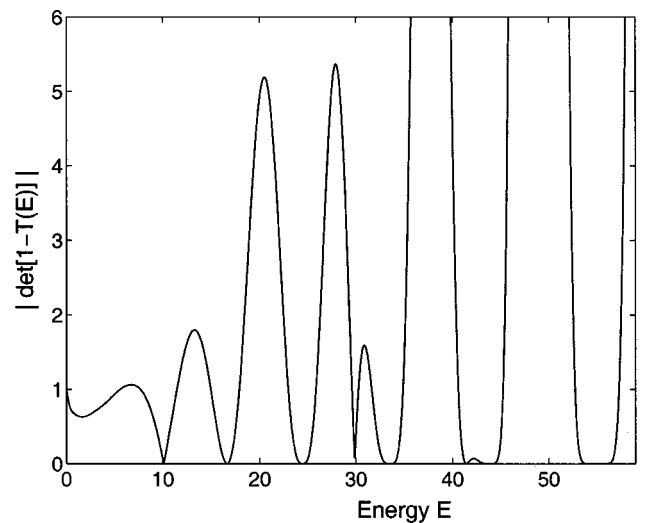


FIG. 7. Absolute value of the Fredholm determinant, $|\det[1 - \mathcal{T}(E)]|$, of the transfer operator $\mathcal{T}(E)$ vs energy E for the half-sphere billiard, where the function $|\det[1 - \mathcal{T}(E)]|$ is dimensionless and the energy E has the unit $\hbar^2/(\mu R^2)$ in Eq. (6).

TABLE I. Ordered semiclassical energies E_n , exact energies E_n^* , the zeros x_n of the Bessel functions, exponents d_n of $|\det[1 - \mathcal{T}(E)]|$ near the zeros E_n , degeneracies d_n^* of E_n^* , and the semiclassical error rate δ_n of the half-sphere quantum billiard, calculated for dimension $N=1715$.

n	E_n	E_n^*	x_n	$d_n = d_n^*$	δ_n (%)
1	10.099	10.095	4.493	1	0.05
2	16.614	16.609	5.763	2	0.03
3	24.424	24.416	6.988	3	0.03
4	29.848	29.838	7.725	1	0.03
5	33.489	33.481	8.183	4	0.02
6	41.372	41.360	9.095	2	0.03
7	43.781	43.768	9.356	5	0.03
8	54.275	54.255	10.417	3	0.04
9	55.280	55.260	10.513	6	0.04
10	59.467	59.450	10.904	1	0.03
11	67.969	67.945	11.657	7	0.04
12	68.524	68.505	11.705	4	0.03
13	75.950	75.930	12.323	2	0.03
14	81.834	81.805	12.791	8	0.04
15	84.093	84.070	12.967	5	0.03
16	93.846	93.820	13.698	3	0.03
17	96.863	96.830	13.916	9	0.03
18	98.958	98.925	14.066	1	0.03
19	100.958	100.919	14.207	6	0.04

quantum billiard, presented in the second column of Table I. The third column lists the exact energies

$$E_n^* = \frac{1}{2} \frac{\hbar^2 x_n^2}{\mu R^2} \quad (6)$$

of the half-sphere quantum billiard (with $R=1$, $\mu=1$, and $\hbar=1$). Therein, $x_n = x(n', l)$, stated in the fourth column, represents the n' th zero of the spherical Bessel function of the first kind, $j_l(x)$, of the l th order. The ordering is such that $x_n < x_{n+1}$ for all possible values of n' and l (see Appendix). The fifth column presents the degeneracies $d_n^* = l$ of E_n^* . The sixth column shows the error rates $\delta_n = (E_n - E_n^*)/E_n^*$ induced by the semiclassical approximation. These errors are bounded by 0.05% from above for $N=1715$ and decrease as N increases. Figure 8 magnifies the function $|\det[1 - \mathcal{T}(E)]|$ in Fig. 7 in the neighborhood of zeros E_n for $n=1, \dots, 6$ (solid curves). The function behaves asymptotically like

$$|\det[1 - \mathcal{T}(E)]| \sim |(E - E_n)^{d_n}| \quad \text{for } E \rightarrow E_n,$$

where the exponent d_n corresponds to the degeneracy of the eigenvalue 1 of the transfer operator $\mathcal{T}(E_n)$, which agrees with the degeneracy d_n^* of the exact quantum energy E_n^* in Table I. The asymptotic polynomials $|(E - E_n)^{d_n}|$ are plotted as dashed curves in Fig. 8.

The consistency of energies E_n and E_n^* and that of degeneracies d_n and d_n^* in the energy regime studied justify the successful application of the transfer operator to these 3D

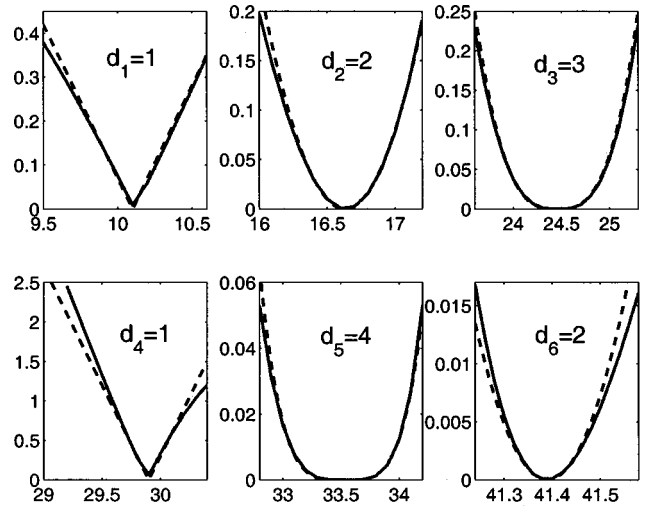


FIG. 8. Asymptotic behavior of $|\det[1 - \mathcal{T}(E)]|$ near zero points E_n (solid curves) and asymptotic polynomials $|(E - E_n)^{d_n}|$ (dashed curves). Units are the same as those in Fig. 7.

systems. Notably, the high dimension, $N=1715$, in the calculation, is used to pursue the upper bound of the semiclassical error as precisely as possible and is not necessary in practical use. In fact, Bogomolny estimated the dimension required to yield a good approximation:

$$N \geq V(E)/(2\pi\hbar)^{k-1},$$

where V denotes the volume of the allowed phase space region of the $(k-1)$ -dimensional section Σ [1]. Accordingly, the required dimensions in the half-sphere billiard are $N=20$ for $E_1=10.099$ and $N=201$ for $E_{19}=100.958$, which are much smaller than $N=1715$.

Figure 9 displays the energy spectra of general lens billiards described by Eq. (5), with various H . The energy spectrum is split into finer spectra due to symmetry breaking induced by the transition from the half-sphere billiard with

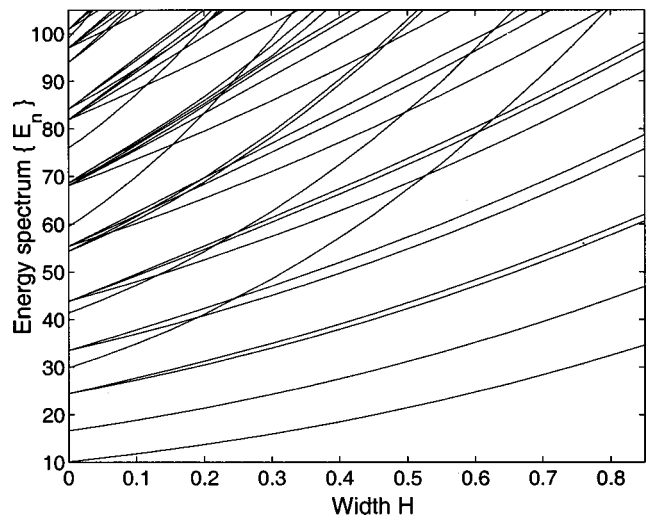


FIG. 9. Energy spectra of lens quantum billiards vs different H in Eq. (5), with the unit $\hbar^2/(2\mu R^2)$, like that in Eq. (6), for E_n and the unit R for H .

$H=0$ to lens billiards with $H>0$. The sums of the split degeneracies for $H>0$ coincide with the nonsplit degeneracy for $H=0$. For example, the degeneracies of the first ten energies for $H=0.75$ are 1, 2, 2, 1, 2, 2, 2, 2, 1, and 1. The sum of the degeneracies of the third and fourth energies for $H=0.75$ is 3, which equals the nonsplit degeneracy 3 of the third energy for $H=0$. It is consistent with the plot in Fig. 9, which shows that E_3 and E_4 for $H=0.75$ are split from E_3 for $H=0$.

V. CONCLUSION

In summary, this work demonstrates how to apply the transfer operator method on the systems with a 2D Poincaré section and 3D trajectories. The geometry studied is the 3D quantum billiards bounded by a flat bottom and an upper surface with $SO(2)$ symmetry, which is motivated by recent observations of the lens-shaped metal clusters. A general strategy for obtaining the energy spectrum of these billiards using classical trajectories, without solving the Schrödinger equation, is presented. The spectra and the corresponding degeneracies of the lens quantum billiards with a varying billiard height, or width H , in the low energy regime are calculated. In the special case of the half-sphere billiard, the zeros E_n of the function $\det[1 - \mathcal{T}(E)]$, determined by the transfer operator method, coincide with the exact quantum energies E_n^* with an error at least less than 0.05%. Furthermore, the degeneracies of the eigenvalue 1 of $\mathcal{T}(E_n)$ coincide with the degeneracies of the exact energies E_n^* . All these results confirm the validity and demonstrate the efficiency of applying the transfer operator method to these 3D systems.

ACKNOWLEDGMENTS

The author would like to thank the National Science Council of the Republic of China, Taiwan, for financially supporting this research under Contract No. NSC 90-2112-M-007-067. S. Gwo and his nanoscience laboratory at Tsing-Hua University are appreciated for their valuable discussions.

APPENDIX

The exact energy eigenvalues of a particle with mass μ bounded inside the sphere of radius R have the same form as that for the half sphere in Eq. (6),

$$E_n^{\text{sphere}} = \frac{1}{2} \frac{\hbar^2 x_n^2}{\mu R^2}.$$

Suppose $x(n', l)$ is the n' th zero of the spherical Bessel function $j_l(x)$ of the l th order, which is listed in Table II, then x_n is the n th smallest value among these zeros $x(n', l)$.

The energy eigenfunction of the sphere is the product of the radial function and the spherical surface function Y_{lm} , e.g.,

TABLE II. Zeros $x(n', l)$ of the spherical Bessel function.

$l \setminus n'$	1	2	3	4	5
0	π	2π	3π	4π	5π
1	4.493	7.725	10.904	14.066	17.221
2	5.761	9.095	12.323	15.515	18.689
3	6.988	10.417	13.698	16.924	20.122
4	8.183	11.705	15.040	18.301	21.525
5	9.356	12.967	16.355	19.653	22.904
6	10.513	14.207	17.648	20.983	24.263
7	11.657	15.431	18.923	22.295	25.603
8	12.791	16.641	20.182	23.591	26.927
9	13.916	17.839	21.428	24.873	28.237
10	15.033	19.026	22.663	26.143	29.535

$$Y_{00}(\theta, \phi) = \frac{1}{2} \sqrt{\frac{1}{\pi}},$$

$$Y_{10}(\theta, \phi) = \frac{\sqrt{3}}{2} \sqrt{\frac{1}{\pi}} \cos(\theta),$$

$$Y_{1\pm 1}(\theta, \phi) = \mp \frac{\sqrt{6}}{4} \sqrt{\frac{1}{\pi}} \sin(\theta) e^{\pm i \phi},$$

$$Y_{20}(\theta, \phi) = \frac{\sqrt{5}}{4} \sqrt{\frac{1}{\pi}} [3 \cos(\theta)^2 - 1],$$

$$Y_{2\pm 1}(\theta, \phi) = \mp \frac{\sqrt{30}}{4} \sqrt{\frac{1}{\pi}} \sin(\theta) \cos(\theta) e^{\pm i \phi},$$

$$Y_{2\pm 2}(\theta, \phi) = \frac{\sqrt{30}}{4} \sqrt{\frac{1}{\pi}} \sin(\theta)^2 e^{\pm 2 i \phi},$$

$$Y_{30}(\theta, \phi) = \frac{\sqrt{7}}{4} \sqrt{\frac{1}{\pi}} \cos(\theta) [5 \cos(\theta)^2 - 3],$$

$$Y_{3\pm 1}(\theta, \phi) = \mp \frac{\sqrt{21}}{8} \sqrt{\frac{1}{\pi}} \sin(\theta) [-5 \cos(\theta)^2 + 1] e^{\pm i \phi},$$

$$Y_{3\pm 2}(\theta, \phi) = \mp \frac{\sqrt{210}}{8} \sqrt{\frac{1}{\pi}} \sin(\theta)^2 \cos(\theta) e^{\pm 2 i \phi},$$

$$Y_{3\pm 3}(\theta, \phi) = \mp \frac{\sqrt{35}}{8} \sqrt{\frac{1}{\pi}} \sin(\theta)^3 e^{\pm 3 i \phi},$$

$$Y_{40}(\theta, \phi) = \frac{3}{16} \sqrt{\frac{1}{\pi}} [35 \cos(\theta)^4 - 30 \cos(\theta)^2 + 3],$$

$$Y_{4\pm 1}(\theta, \phi) = \mp \frac{\sqrt{5}}{8} \sqrt{\frac{1}{\pi}} \sin(\theta) e^{\pm i \phi},$$

$$\times \{12 \cos(\theta)^3 - 9[1 - \cos(\theta)^2] \cos(\theta)\},$$

$$Y_{4\pm 2}(\theta, \phi) = \mp \frac{\sqrt{10}}{16} \sqrt{\frac{1}{\pi}} \sin(\theta)^2 [21 \cos(\theta)^2 - 3] e^{\pm 2i\phi},$$

$$Y_{4\pm 3}(\theta, \phi) = \mp \frac{3\sqrt{35}}{8} \sqrt{\frac{1}{\pi}} \sin(\theta)^3 \cos(\theta) e^{\pm 3i\phi},$$

$$Y_{4\pm 4}(\theta, \phi) = \frac{3\sqrt{70}}{32} \sqrt{\frac{1}{\pi}} \sin(\theta)^4 e^{\pm 4i\phi}.$$

The energy for the sphere has degeneracy $2l+1$, because of the relation $-l \leq m \leq l$ with $l \geq 0$. However, only the odd functions Y_{lm} in θ listed above, which disappear on the equator plane $\theta = \pi/2$, contribute to the wave functions for the

half sphere, e.g., Y_{10} , Y_{20} , $Y_{2\pm 2}$, Y_{30} , $Y_{3\pm 2}$, etc.; that is, the energy form for the sphere and for the half sphere are the same, as in Eq. (6). Nevertheless, due to the symmetry breaking from $SO(3)$ for the sphere to $SO(2)$ for the half sphere, the degeneracies of the energies are reduced from $2l+1$ to l . The counting of the n th smallest energy begins with $l \geq 0$ for the sphere and with $l \geq 1$ for the half sphere, because the only one function $Y_{00}(\theta, \phi)$ for $l=0$ is not an eigenfunction for the half sphere, since it does not satisfy $Y_{00}(\pi/2, \phi) = 0$. Therefore, the n th energy E_n^* in Table I comes from the n th smallest value among all $x(n', l)$ with $l \geq 1$ in Table II. The (n', l) values of the first seven smallest energies E_n^* are (1,1), (1,2), (1,3), (2,1), (1,4), (2,2), (1,5) with the corresponding degeneracies $l=1, 2, 3, 1, 4, 2, \text{ and } 5$.

-
- [1] E.B. Bogomolny, *Nonlinearity* **5**, 805 (1992).
 [2] M. Brack and R.K. Bhaduri, *Semiclassical Physics* (Addison-Wesley, Reading, MA, 1997).
 [3] M.C. Gutzwiller, *Chaos in Classical and Quantum Mechanics* (Springer, New York, 1990).
 [4] H. Primack and U. Smilansky, *Phys. Rev. Lett.* **74**, 4831 (1995); *Phys. Rep.* **327**, 1 (2000).
 [5] B. Lauritzen, *Chaos* **2**, 409 (1992).
 [6] B. Hu, B. Li, and D.C. Rouben, *J. Phys. A* **32**, 5419 (1999).
 [7] T. Szeredi, J.H. Lefebvre, and D.A. Goodings, *Nonlinearity* **7**, 1463 (1994).
 [8] D.A. Goodings and N.D. Whelan, *J. Phys. A* **31**, 7521 (1998).
 [9] N.C. Snaith and D.A. Goodings, *Phys. Rev. E* **55**, 5212 (1997).
 [10] C.-H. Chang, *Phys. Rev. E* **66**, 056202 (2002).
 [11] T. Szeredi, J.H. Lefebvre, and D.A. Goodings, *Phys. Rev. Lett.* **71**, 2891 (1993).
 [12] P. Tong and D.A. Goodings, *J. Phys. A* **29**, 4065 (1997).
 [13] M.R. Haggerty, *Phys. Rev. E* **52**, 389 (1995).
 [14] E.B. Bogomolny and M. Caroli, *Physica D* **67**, 88 (1993).
 [15] D. Bimberg, M. Grundmann, and N.N. Ledentsov, *Quantum Dot Heterostructures* (Wiley, West Sussex, UK, 1999).